Atmospheric Temperature and Absolute Humidity Profiles over the Beaufort Sea and Amundsen Gulf from a Microwave Radiometer

LAUREN M. CANDLISH, RICHARD L. RADDATZ, MATTHEW G. ASPLIN, AND DAVID G. BARBER

Centre for Earth Observation Science, University of Manitoba, Winnipeg, Manitoba, Canada

(Manuscript received 11 December 2010, in final form 22 February 2012)

ABSTRACT

A Radiometrics MP-3000A microwave radiometric profiler (MWRP) provided high temporal resolution atmospheric profiles for temperature and absolute humidity up to 10 km, while 113 radiosondes were launched (and 68 were used in the analysis) over sea ice and the open ocean during the 2008 Circumpolar Flaw Lead System Study and the 2009 ArcticNet Cruise in the western Canadian High Arctic. The profiles were categorized by season and by the underlying sea ice concentrations. The MWRP was validated against the radiosonde data, focusing on the lower 2 km, which are generally influenced by the nature of the underlying surface. Root-mean-square (RMS) differences for temperature averaged 1.79 K through the lowest 2 km for the winter season, 1.81 K for spring, 2.51 K for summer, and 2.47 K for fall. Average biases of +0.99, +1.19, +2.13, and +2.08 K, respectively, indicate that the MWRP measurements were colder than the raobs for the lower 2 km. The RMS difference for absolute humidity averaged 0.25 g m^{-3} in the lowest 2 km during the winter season, 0.32 g m^{-3} for spring, 0.74 g m^{-3} for summer, and 0.37 g m^{-3} for fall. Average biases of +0.08 g m^{-3} for profiles over $^{9}/_{10}$ths and $^{10}/_{10}$ths sea ice concentration, +0.26 g m^{-3} for profiles over $^{2}/_{10}$ths–$^{8}/_{10}$ths concentrations, and +0.16 g m^{-3} over $^{0}/_{10}$ths and $^{1}/_{10}$th concentrations indicated that the MWRP measurements were slightly drier than the raobs for the lower 2 km. An estimate of the vertical resolutions indicated that it was as coarse as the height measured; however, the structure apparent in the profiles and the verification statistics suggest a higher vertical resolution, at least in the lowest 2 km.

1. Introduction

In recent years, there has been an increased interest in accurately modeling Arctic weather and climate. The Arctic is an understudied area that contributes greatly to the global circulation and radiation budget. The Arctic climate is changing with air temperatures increasing 4 or 5 K in the western Canadian Arctic and Alaska (Turner et al. 2007), in conjunction with an increase in ocean temperatures causing reductions in sea ice thickness (Rothrock et al. 1999), sea ice volume (Kwok and Cunningham 2010), average age of ice (Maslanik et al. 2007, 2011), and an increasing melt season length (Markus et al. 2009). These changes in sea ice cover can release large heat and moisture fluxes into the Arctic atmosphere throughout the cold season, thus modifying the regional boundary layer climate. To better understand the changes being observed in the Arctic, reliable in situ data are required. The use of a Radiometrics profiling radiometer on board a ship in the Arctic is a new and unique method that provides high temporal profiles of the atmospheric temperature and humidity profiles, as well as cloud-base heights, over a large range of ocean and sea ice surfaces.

Several large research projects have been undertaken to achieve a better understanding of the three-dimensional structure of the Arctic atmosphere and its seasonal patterns. These projects included the Circumpolar Flaw Lead System Study (CFL) and the ArcticNet Cruise. The CFL project, from October 2007 to August 2008, was an overwintering field campaign in the Amundsen Gulf (70.5°N, 124.0°W) supported by the Canadian Coast Guard Ship (CCGS) *Amundsen*, Canada's research icebreaker (Barber et al. 2010). The 2009 ArcticNet Cruise occurred from July to November 2009 in the Beaufort Sea, and was also supported by the CCGS *Amundsen*. The Circumpolar Flaw Lead Study and the ArcticNet Cruise 2009 provided a unique opportunity for the validation of a mobile Radiometrics profiling

Corresponding author address: Lauren M. Candlish, Centre for Earth Observation Science, University of Manitoba, Winnipeg, MB R3T 2N2, Canada.
E-mail: lcandlish@gmail.com

DOI: 10.1175/JTECH-D-10-05050.1

radiometer during all seasons in the western Canadian Arctic. Microwave radiometric profilers (MWRPs) have been operated and tested at a variety of locations around the world, including Linkenholt, United Kingdom; Lindenberg, Germany; Payerne, Switzerland; and Colorado, Alabama, Oklahoma, Kansas, Washington, and Alaska in the United States.

Gaffard et al. (2008) found that in Likenholt the radiometer profiles decreased in accuracy with height. Using data from Lindenburg and Lamont, Washington, Ware et al. (2003) observed that the microwave radiometer profiles are smoother than radiosonde profiles; this is a result of the microwave radiometer giving volumetric measurements while the radiosonde gives point measurements with higher vertical resolution. Knupp et al. (2009) determined that MWRP's are capable of providing considerable detail on the rapidly changing thermodynamic structure of transitioning boundaries, including cold fronts, gust fronts, bores, and gravity waves. A benefit of the MWRP over radiosondes is the high temporal resolution that can detect the passage of such boundaries associated with thermodynamic changes that occur on very short time scales, on the order of 1–10 min, which is far too short to be captured by radiosondes.

This paper examines data from a Radiometrics MP-3000A MWRP in the Amundsen Gulf and Beaufort Sea. Field data were collected over sea ice and the open ocean in the western Canadian High Arctic. Throughout the CFL project, 65 weather balloons carrying Vaisala radiosondes (raobs) were launched while the Radiometrics microwave profiling radiometer produced nearly continuous vertical profiles of the atmosphere from the surface to 10 km from November 2007 until July 2008. The second field campaign supported by ArcticNet on board the CCGS *Amundsen* provided an additional 48 radiosonde profiles plus continuous microwave profiles from July until November 2009.

The objective of this paper was to determine how reliable the MWRP was when mounted on board a mobile ship in the High Arctic. The first part of this objective was addressed by statistically comparing coincident radiosonde measurements to the MWRP measurements taken for temperature and absolute humidity from the surface to 10 km in height. A second objective was to investigate whether the performance of an MWRP, when profiling the boundary layer of the Arctic atmosphere over the western Canadian Arctic, varies based on surface sea ice conditions.

2. MWRP description

The Radiometrics MP-3000A microwave profiling radiometer provides high temporal resolution (≈1 min) atmospheric profiles for temperature (K), absolute humidity (g m^{-3}), and liquid water (g m^{-3}) up to 10 km. The MWRP on board the CCGS *Amundsen* was mounted behind the bridge near the smokestack (Fig. 1). The MWRP uses passive microwave radiometry for water vapor and temperature profiling. The instrument contains sensors to measure surface pressure, surface temperature, and surface relative humidity. The MWRP also contains a zenith-pointing infrared radiometer (9.6–11.5 μm) to provide the cloud-base temperature, and by inference from the retrieved temperature profile, cloud-base altitude. The temperature and humidity profiles were processed in real time, giving nearly continuous monitoring of the lower troposphere, interrupted only by accumulation of liquid water on the radome during moderate to heavy precipitation.

FIG. 1. The MWRP mounted on board the CCGS *Amundsen*.

Solheim et al. (1998), Guldner and Spankuch (2001), Ware et al. (2003), and Gaffard et al. (2008), provide complete descriptions of the radiometric profiling of temperature and water vapor, so only a brief description is provided. The MP-3000A views atmospheric radiances from the zenith direction in 22 microwave channels. The 8 channels between 22 and 30 GHz provide information on the water vapor profiles, while the 14 channels in the oxygen band (51–59 GHz) provide information on the atmospheric temperature profile. The radiometer has a viewing angle of 2°–3° in the oxygen band and 5°–6° in the water vapor band, giving an inverted cone observation (Ware et al. 2003). The water vapor profiling channels are calibrated hourly with tipping curves (Guldner and Spankuch 2001). An external liquid nitrogen target is used to intermittently calibrate the temperature channels. All 22 channels perform a relative calibration every 5 min by viewing an internal blackbody target.

The MWRP provided temperature and humidity values that are volumetric measurements at 50-m intervals for 0–0.5 km, 100-m intervals for 0.5–2 km, and 250-m intervals for 2–10 km. The values are derived from microwave brightness temperatures using the Radiometric's neural network retrieval and radiative transfer model. The neural network was trained on historical radiosonde data from the upper air station in Inuvik, Northwest Territories, Canada (68.30°N, 133.47°W). While the location of Inuvik is approximately 100 km from the coastline, it is the closest location that has a sufficient number (thousands) of historical radiosondes to train the neural network.

The accuracy of the MWRPs has mainly been evaluated against radiosondes at midlatitude continental locations. Although radiosondes are the standard for atmospheric profiling of temperature and humidity, there are inherent measurement errors in radiosondes, about 0.5 K for temperature and 10% for relative humidity (Pratt 1985; Schmidlin 1988; Miloshevich et al. 2006). These measurement errors and the drift of the ascending balloon relative to the zenith, makes them less than ideal references (Guldner and Spankuch 2001). Hewison (2007) evaluated the root-mean-square (RMS) differences between radiosonde and radiometric measurements mainly based on data from Camborne, United Kingdom, and found that the RMS difference for temperature was 0.6 K near the surface, increasing to 1.5 K at 3.3 km. For absolute humidity the RMS difference was 0.5 g m^{-3} near the surface, increasing to 1.1 g m^{-3} between 1 and 2 km. For Oklahoma and Kansas, and Barrow, Alaska, Liljegren et al. (2001) found RMS differences of 1–2 K for temperature. For absolute humidity, the RMS differences were 1–2 g m^{-3} at the Oklahoma and Kansas sites, and 0.5 g m^{-3} for Barrow where the vapor density is much smaller, averaging 1 g m^{-3}. Cimini et al. (2007) found that the brightness temperatures from the oxygen bands of an MWRP compared reasonably well with the values obtained from a 26-channel ground-based scanning radiometer, both deployed at Barrow for the Arctic Winter Radiometeric Experiment (in 2004).

Hewison (2007) gives the observation error for simulated results from a TP/WVP-3000 microwave radiometer. They found that for the water vapor band, the observational error for the brightness temperature was in the range of 1.04–1.19 K. In the oxygen band, channels at 53.85–58.8 GHz were found to have observational errors from 0.14 to 0.67 K. The channels at 51.25 and 52.28 GHz were found to have 2.04 and 1.62 K, respectively. The MP-3000A MWRP has an environmental operating range from 232 to 307 K, and operational capabilities for winds speeds of up to 30 m s^{-1} (Radiometrics 2008).

Because the neural network was trained using land-based radiosondes there was some concern that the microwave radiometer profiles would have a bias when it was located on a ship in a marine environment. However, in the Arctic marine environment the sea ice cover can act as a barrier limiting the exchange of latent and sensible heat, in addition to the exchange of water vapor between the ocean and atmosphere (Barry et al. 1993). Nevertheless, new ice with thickness of 0–0.4 m still allows heat fluxes of one and two orders of magnitude larger than through thicker ice (Maykut 1978). While sea ice can reduce the amount of latent and sensible heat being transferred between the ocean and the atmosphere, this is very dependent on the time of year and sea ice conditions. Increased amounts of sea ice may reduce the inaccuracies of the MWRP caused by neural network using radiosondes launched over land.

The MWRP viewed in the zenith may be sensitive to the pitch and roll motions of the ship. There may be a greater error relative to land-based locations. During the winter season of CFL, the CCGS *Amundsen* was operating in drift mode, parked in large ice floes for several days, repositioning occasionally to stay within the study region. The large ice floes and 9+ 10ths coverage throughout the basin dampen ocean swells, likely reducing the error resulting from the pitch and roll of the ship.

All 22 channels of the microwave profiler view an internal blackbody to perform a relative calibration every 5 min. This internal blackbody has a bias that is accounted for in the processing of the brightness temperatures to the temperature and humidity profiles. Brightness temperature observations using ventilated and unventilated blackbodies show systematic differences on the order of

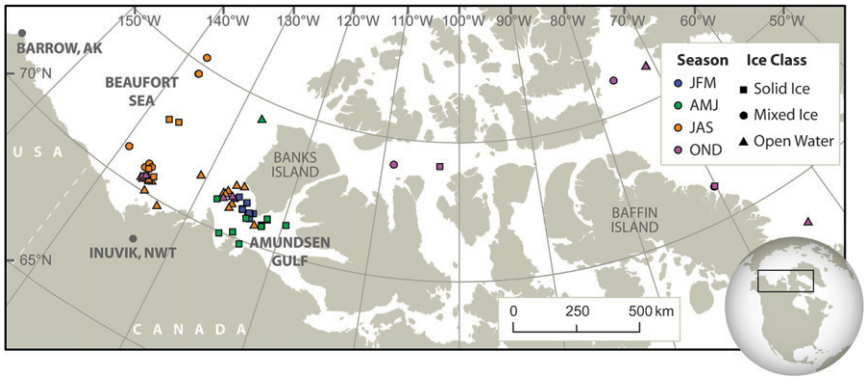

FIG. 2. A map of the study region. Locations of the radiosonde profiles are shown; the color represents the season it was launched: JFM (blue), AMJ (green), JAS (orange), and OND (pink). The shape of the symbol represents the sea ice concentration class present at the time of the launch: solid ice (square), mixed ice (circle), and open water (triangle). Inuvik, the location for the MWRP training radiosondes (dark gray), and Barrow, the location of the closest MWRP and radiosonde site (dark gray), are shown.

0.5 K (R. Ware, Radiometrics, 2012, personal communication). The estimated internal blackbody bias may cause a cold bias in the temperature profiles. Because neural networks are nonlinear, retrieval sensitivity to offsets is variable and may also be dependent on weather conditions, climatology, and the radiometer calibration.

The MWRP aboard the CCGS *Amundsen* was calibrated using an external liquid nitrogen target. The recommended calibration schedule is 6 months. During 2008 and 2009 the calibrations were performed every 2–4 months. The calibrations files show a drift of less than 1% for each channel between the calibrations. This indicates that the calibrations were performed at a greater frequency than required and the instrument was well calibrated during the field seasons (R. Ware, Radiometrics, 2012, personal communication).

3. Data

Out of the 113 radiosondes launched, a total of 68 profiles, comprised of 36 from the CFL project (January–July 2008) and 32 from the ArcticNet Cruise (July–November, 2009), were used in the comparisons. When launched, the radiosondes attached to a weather balloon drift with the wind and deviate from the zenith as viewed by an MWRP. Thus, profiles were rejected if the raobs went out of range before reaching an altitude of 10 km or went in and out of range within the lower 10 km. The Vaisala RS92-SGPD radiosondes took 45 min–1 h for ascent. Furthermore, approximately 25% of the launches occurred while the ship was in transit. To account for the drift of the balloons as well as the time for the balloon to ascend, the MWRP data were averaged over 1 h, starting at the time of launch. Figure 2 shows the locations of the 68 comparable raobs and microwave radiometer profiles, as well as Inuvik and Barrow.

During CFL, an issue with the firmware installed on the base station for the radiosondes caused frequent drops in relative humidity readings. This impacted the absolute humidity values because they were calculated using the Clausius–Clapeyron equation from relative humidity. The firmware issue caused the relative humidity to rapidly decrease down to 10% or less and then rapidly increase back up to its prior value. The relative humidity data were corrected using linear interpolation. Data were rejected if erroneous relative humidity readings could not be distinguishable from natural decreases in relative humidity. As well, the entire radiosonde profile was rejected if either the rapid decreases and increases in relative humidity were very frequent, occurring for more than 40% of the time, or they occurred for longer than 90 s.

The CCGS *Amundsen* is based out of Quebec City, Quebec, Canada. While traveling through the Northwest Passage to go to and from the Beaufort Sea, a total of seven profiles were collected. Data collected in transit have been included in the dataset, because the profiles were not outliers when the MWRP was compared to the raobs.

With the MWRP neural network being trained with thousands of radiosondes from Inuvik, the comparison of data from Inuvik is essential. Established in the 1970s, the Environment Canada upper air station at Inuvik operates year-round, launching weather balloons twice daily at 0000 and 1200 UTC. The 68 radiosonde profiles from the ship were compared with those launched at the same time from Inuvik—the training site. The dates and times were chosen as close as possible to the time of launch on board the CCGS *Amundsen*.

The Atmospheric Radiation Measurement (ARM) program has a site in Barrow. The Barrow site has a first-generation Radiometrics MWRP that ran continuously through 2008 and 2009, with interruptions only for calibration and maintenance. The ARM site also launched two radiosondes daily during 2008 and 2009. The accuracy of the ship-based MWRP was assessed relative to the closest validated MWRP. Microwave radiometric profiles from the ARM site at Barrow were compared to 68 radiosondes from that location to set a standard for the ship-based profiles. The dates and times of these profiles were less than 6 h from the dates and times of the profiles used from the ship.

The ship-based atmospheric profiles were grouped by season, with winter being defined as January–March (JFM), spring as April–June (AMJ), summer as July–September (JAS), and fall as October–December (OND). The standard deviations of the raobs at each MWRP level were calculated for each season (Fig. 3). The standard deviations of the Inuvik radiosondes were also calculated for each season (Fig. 3).

Figure 4 shows that the mean and range of the temperature for Inuvik were generally greater than at the ship's location. The standard deviation (Fig. 3) also showed differences between Inuvik and the ship, with the standard deviation of Inuvik being generally greater from the surface to approximately 8 km, with the exception of JAS, where the standard deviation of Inuvik was less than the *Amundsen*'s location from 1 to 8 km.

Figure 4 shows that the mean and range of the absolute humidity for Inuvik were generally greater than at the ship's location. The standard deviation (Fig. 3) also showed differences between Inuvik and the ship. While only the surface data are described below, it should be noted that the differences between the ship-based and Inuvik profiles generally decreased with height.

For JFM the surface temperatures measured by the ship-based raobs ranged from 240.5 to 258.9 K, with a mean temperature of 250.1 K and a standard deviation of 6.4 K. Similarly, Inuvik had surface temperatures ranging from 234.5 to 266.5 K, with a mean of 251.5 K and a standard deviation 10.3 K. During JFM the surface temperatures were always well below freezing and the CCGS *Amundsen*, at the times of the radiosonde launches, generally had thick first-year ice in the immediate vicinity of the ship. Ten of the radiosondes were launched in areas where the ice thickness was greater than 1.0 m, 2 radiosondes were in areas greater than 0.7 m, and two profiles were taken during transit with the ice thickness unknown. In AMJ the surface temperatures measured by the ship-based raobs had a range of 248.1–273.0 K with a mean temperature of 264.0 K and a standard deviation of 7.7 K. In this period, the surface temperatures reached the melting point of sea ice, which caused ponds to develop on the sea ice surrounding the ship. Inuvik's temperatures ranged from 253.7 to 283.8 K, with a mean of 268.4 K and a standard deviation of 9.4 K. JAS had a range from 269.4 to 290.2 K, with a mean of 275.5 K and a standard deviation of 4.5 K. The sea ice concentration varied greatly during JAS; however, with temperatures consistently above the freezing point mainly open water surrounded the ship. In Inuvik, the temperatures were generally warmer with a mean of 284.0 K, nearly 10° warmer than the ship, and a range from 267.3 to 296.8 K. The standard deviation of Inuvik was 8.3 K, again greater than the ship's. OND had ship-based surface temperatures ranging from 258.9 to 272.8 K, with a mean of 265.2 K and a standard deviation of 4.8 K. For OND the temperatures dropped below the freezing point, resulting in new first-year ice being formed. The mean temperature in Inuvik was approximately the same as the ship: 264.1 K, with a range from 251.9 to 271.7 K and a standard deviation of 7.0 K. Sea ice concentrations varied greatly during the study period from the open ocean ($^{0}/_{10}$ths) to consolidated ($^{10}/_{10}$ths) ice. With such varied ice concentrations during the course of the seasons, the ship-based raobs and MWRP profile datasets cover a broad range of weather conditions.

The neural network was trained using radiosondes launched from the Environment Canada upper air station at Inuvik. Five years' worth of Inuvik radiosondes from 2002 to 2006 were grouped into the seasons JFM, AMJ, JAS, and OND. The Mann–Whitney two-sample difference test was used to compare the Inuvik radiosondes to the radiosondes launched aboard the CCGS *Amundsen* during 2008 and 2009 over the Beaufort Sea. The Mann–Whitney test showed that the temperature and humidity profiles collected during JFM of 2008 were statistically similar to the historical Inuvik raobs for all height values, except for heights nearing 10 km. In general, the temperature and humidity profiles collected during AMJ 2008 were not statistically similar to the historical Inuvik raobs. JAS profiles were not as clearly defined; the temperature profiles from 2008 and 2009 were not statistically similar from the surface to about 2 km, but from 2 to 10 km the temperatures were statistically similar. The absolute humidity profiles in JAS were not statistically similar for the entire profile. In OND the temperature profiles were statistically similar only near the surface from 200 m to 1.25 km and in the upper profile from 7.5 to 8.75 km. The humidity profiles during OND were statistically similar from the surface to 8.5 km; above 8.5 km the two datasets were not statistically similar.

The Mann–Whitney two-sample difference test shows that the data collected over the Beaufort Sea were

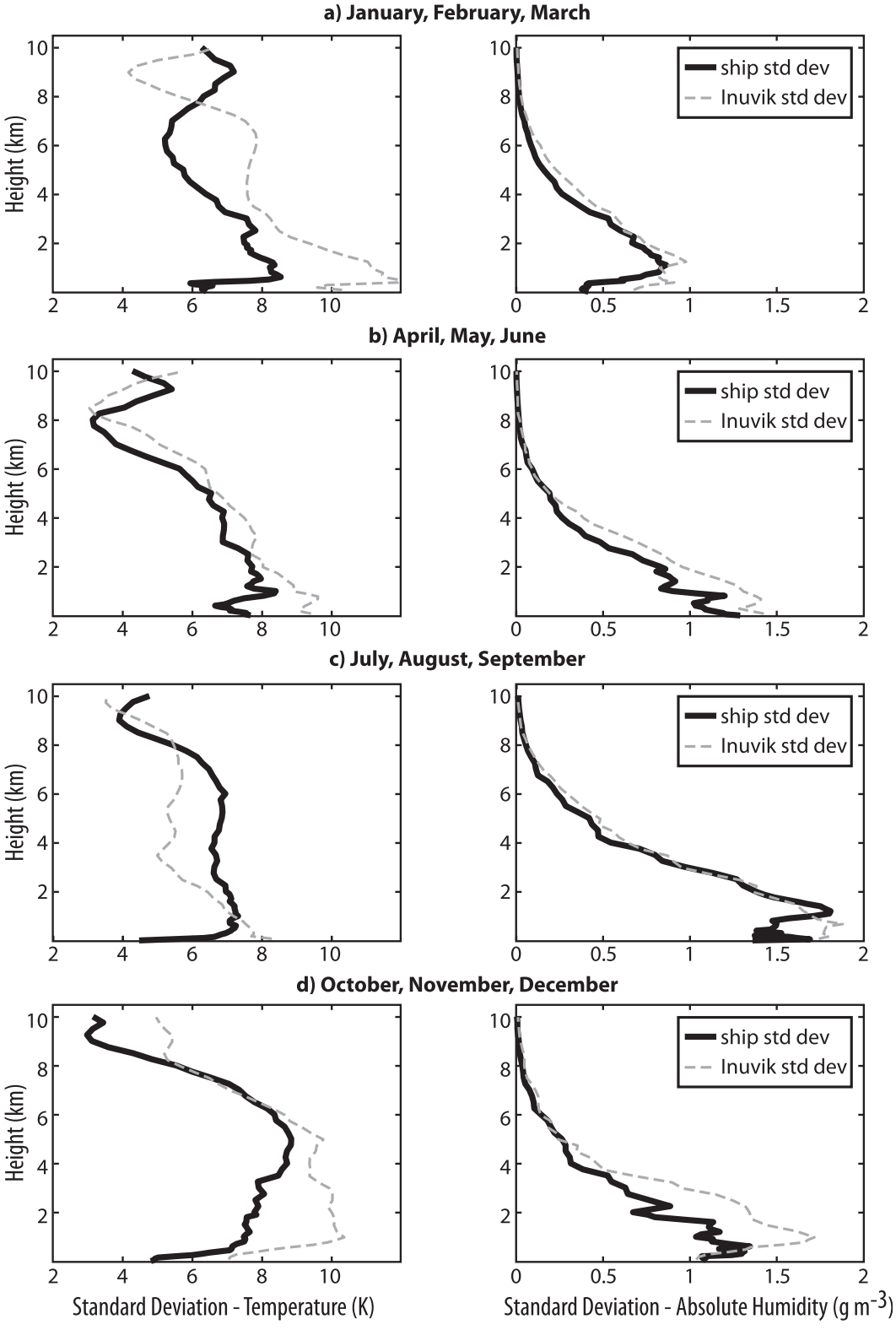

FIG. 3. The standard deviation vs height (km) for (left) temperature and (right) absolute humidity. The standard deviation for the ship was calculated from the raobs used in the comparisons (thick black solid line). The standard deviation for Inuvik was calculated using raobs at the same date as those on the ship (thin dashed gray line). The standard deviation of Inuvik was generally greater than the ship.

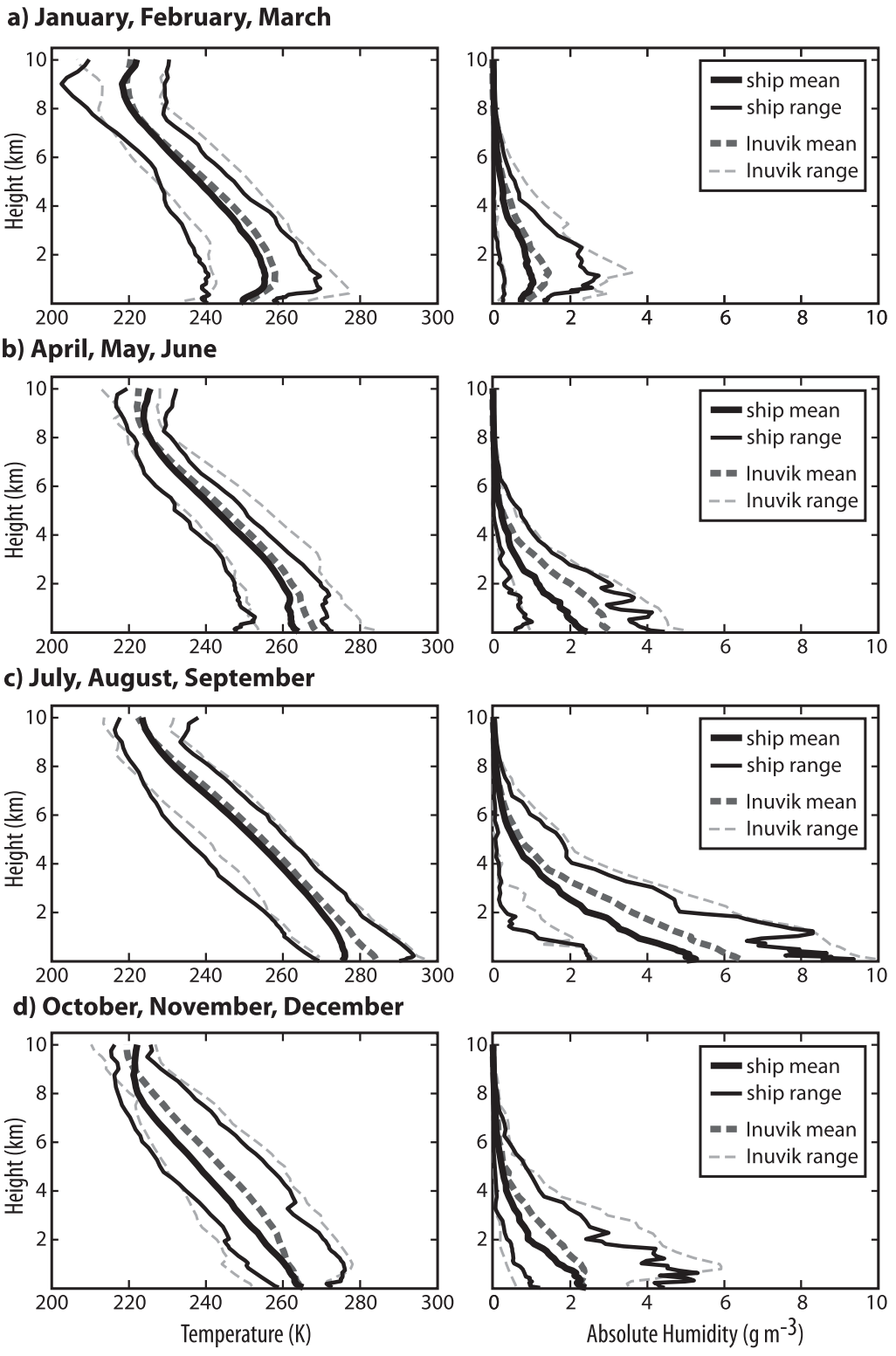

FIG. 4. The mean atmospheric profile vs height (km) for (left) temperature and (right) absolute humidity. The mean was calculated from the raobs used in the comparisons. The data were categorized by seasons [(a) JFM, (b) AMJ, (c) JAS, and (d) OND]. The mean and range for Inuvik is shown, with the mean calculated using raobs launched at the same date as those on the ship (thin dashed gray line). During 2008–09 Inuvik generally had a greater range with warmer temperatures.

generally not statistically similar to the historical Inuvik data, with the exception of JFM and OND, when the Beaufort Sea had high concentrations of sea ice present. This further indicates that the MWRP bias is likely affected by the neural network being trained with historical Inuvik radiosonde data.

To summarize the temperature and moisture characteristics of the atmosphere over the study region, the radiosonde data were divided into seasons. There were a total of 68 profiles for comparison over the study periods: 14 in JFM, 11 in AMJ, 30 in JAS, and 13 in OND.

To examine more closely the impact of the sea ice concentration surrounding the CCGS *Amundsen* on the temperature and moisture characteristics of the atmospheric boundary layer profiles, the raobs were also divided into three categories, regardless of season, based on the concentrations of sea ice. Open water was defined as $^{0}/_{10}$ths and $^{1}/_{10}$th, mixed sea ice cover as $^{2}/_{10}$ths to $^{8}/_{10}$ths, and close pack ice cover as $^{9}/_{10}$ths and $^{10}/_{10}$ths. The sea ice concentrations were visual observations by the ships officers or ice observers and were subjective. Because the visual horizon is about 25 km, these observations represent the sea ice concentrations within 25 km of the CCGS *Amundsen*. By dividing the data into only three sea ice concentration categories some of the subjectivity was eliminated, because $^{2}/_{10}$ths to $^{8}/_{10}$ths are the most open to interpretation and all of these observations were grouped together into one category. Poor visibility can also cause a problem for observing ice cover. No poor visibility occurred during the times when radiosondes were launched, and thus no data were discarded due to this limitation.

The mean atmospheric profiles, measured by the raobs, were calculated for each season (Fig. 4) and sea ice concentration category (Fig. 5). The mean temperature profile for JFM shows a strong temperature inversion with a lapse rate of 5.0 K km^{-1} in the bottom 1 km (Fig. 4a). During JFM the sea ice concentrations at the time of the raobs were either $^{9}/_{10}$ths or $^{10}/_{10}$ths. When the data were grouped by sea ice concentrations the average profile for close pack ice, $^{9}/_{10}$ths or $^{10}/_{10}$ths, showed only a very weak temperature inversion with a lapse rate of 2.1 K km^{-1} (Fig. 5a). The close ice pack category includes profiles that were taken during each of the four seasons, which led to the differences from JFM in the mean temperature and humidity profiles. The average surface temperature during JFM was 10 K less than the average surface temperature of the close ice pack category. The mean absolute humidity during JFM was less than 1 g m^{-3} from the surface up to 2 km, whereas for close ice pack the mean absolute humidity was 2 g m^{-3} at the surface and reduces to 1.5 g m^{-3} at 2 km. The mixed ice category has seven profiles during JAS and four from OND. As a result, the mean temperature profile for mixed ice was approximately 5 K warmer than for OND and 5 K cooler than for JAS. Similarly, the mean humidity profile for mixed ice had less moisture at the surface than JAS and more moisture than OND. The open water group, $^{0}/_{10}$ths or $^{1}/_{10}$th, consists of 18 profiles during JAS, with 1 profile in AMJ and 7 from OND. The resulting mean temperature profile was slightly cooler than JAS; similarly, the mean absolute humidity profile is slightly drier.

4. Validation with radiosondes

To validate the microwave profiler against radiosondes several statistical analysis were performed. Section 4a discussed the Wilcoxon match pair test, performed on the MWRP and the raobs, which determined if the two datasets were statistically similar. Section 4b analyses the root-mean-square difference and bias of the MWRP minus the raobs. Section 4c compares the RMS difference and bias from the ship-based MWRP and raobs to an MWRP stationed at Barrow. The Mann–Whitney two-sided rank sum test was performed on the RMS difference (bias) between the ship and Alaska for each season to determine if the RMS difference (bias) is statistically similar to the MWRP located at Barrow. Section 4d analyses the frequency distribution of the case-to-case differences of the MWRP and the raobs. The frequency distribution shows if the data have a systematic or random error.

a. Wilcoxon match pair test

The Wilcoxon match pair nonparametric test was calculated on the raobs and MWRP for the ship-based profiles for each height level and season (Fig. 6). The test is designed to run on small sample sizes that are not normally distributed. The test gave p values for each of the 58 MWRP height levels, with a p value less than (greater than) 0.05 indicating that the MWRP data and the raob data are statistically similar (dissimilar), meaning there is statistical significance that the distributions of the MWRP and raobs are similar (dissimilar) at the height level.

For temperature the MWRP is statistically similar to the raobs for the midheights, approximately 0.25–6 km for JFM and AMJ, 1.2–9.5 km for JAS, and 0.25–9 km for OND. The MWRP is statistically different near the surface, with less than 0.25 km for JFM, AMJ, and OND; AMJ is also statistically different near 1 km, and JAS is statistically different for the surface to 1.2 km. For JFM and AMJ the MWRP and raobs are statistically different at heights between 6 and 10 km; however, JAS is statistically different at heights greater than 9.5 km and OND is statistically different at heights greater than 9 km.

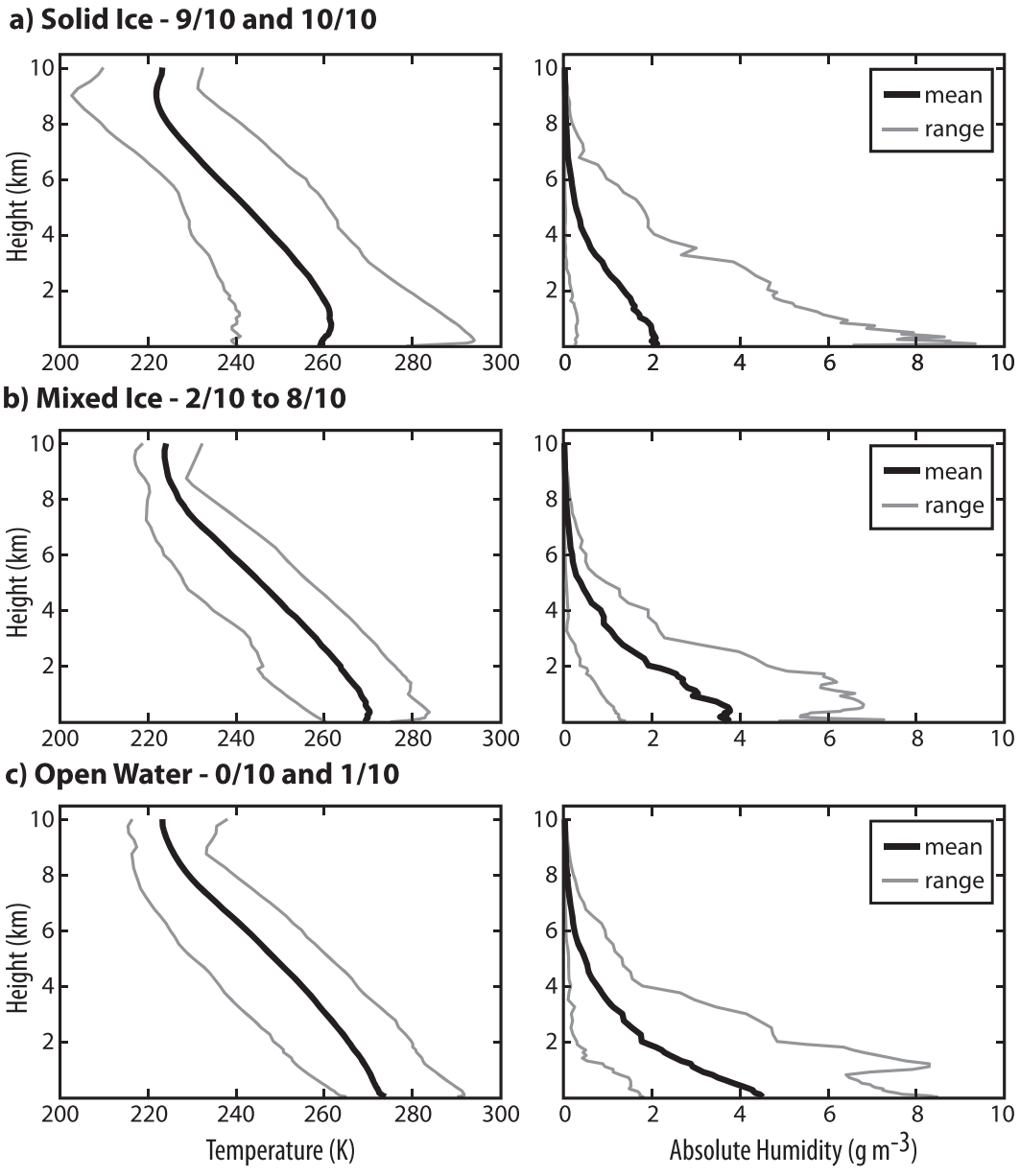

FIG. 5. The mean atmospheric profile vs height (km) for (left) temperature and (right) absolute humidity. The mean was calculated from the raobs used in the comparisons. The data were categorized by sea ice concentrations.

For absolute humidity, the Wilcoxon test indicated that the MWRP and the raobs are statistically different at more height levels than for temperature. For JFM, AMJ, and OND the MWRP and the raobs are generally statistically similar below 0.5 km; however, for JAS the two are generally statistically different for up to 6.5 km.

When comparing the MWRP data to the raobs it is important to note that when the two datasets were statistically similar the MWRP and raobs are measuring from the same population. A bias may still be present in the MWRP data, but if the raobs are statistically similar to the MWRP, then both instruments may have a similar bias. This indicates that for temperature, above 200–250 m to approximately 5–9 km, the MWRP and raobs are statistically similar and therefore are likely measuring the same population, with the exception of JAS where the surface to approximately 1.2 km are statistically different. For absolute humidity, however, the data were generally statistically different, indicating that the MWRP and raobs were measuring from different populations. This may be due, in part, to the radiosonde's

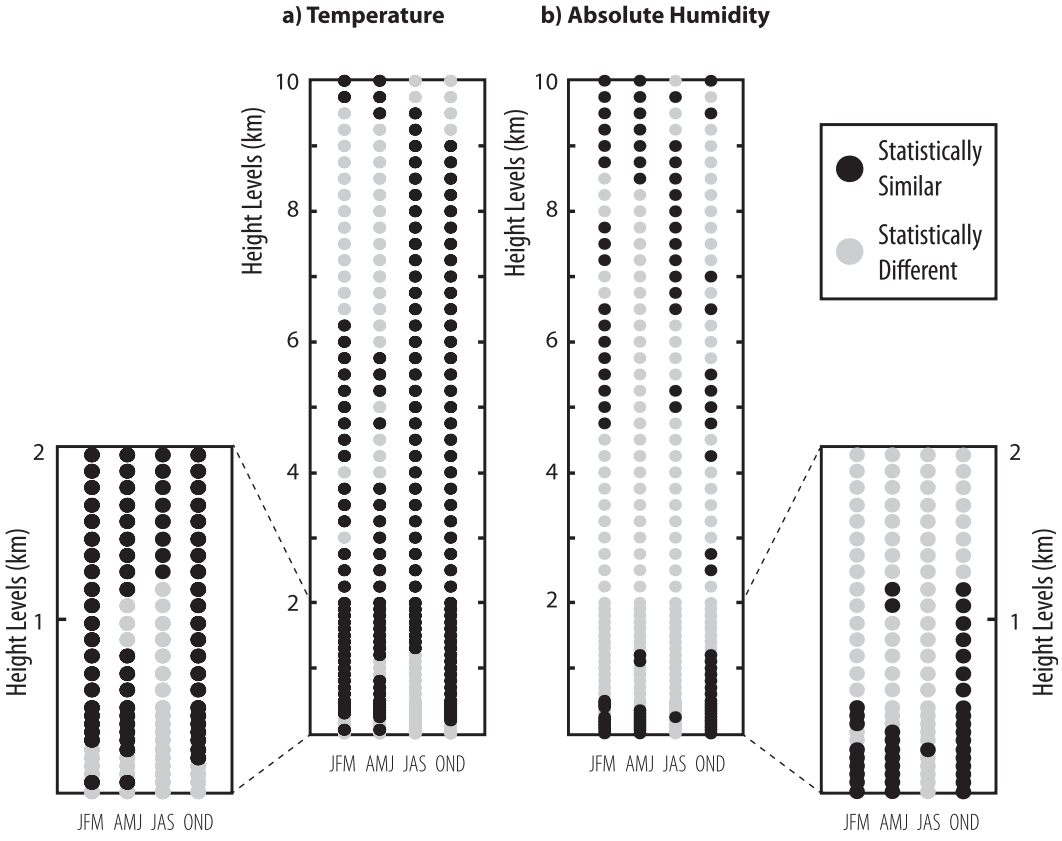

FIG. 6. The Wilcoxon match pairs nonparametric test calculated on the MWRP data and the raob data. A p value of less than 0.05 indicates the height level is statistically similar (black points). A p value of greater than 0.05 indicates the height level is statistically different (gray points).

firmware malfunction, causing the rapid decreases in relative humidity.

b. Root-mean-square difference and bias

The RMS difference and bias were calculated for each of the MWRP levels and grouped by season (Fig. 7). The RMS difference and biases were calculated as the raobs minus the MWRP. The RMS difference and bias profiles for temperature (left-hand column, Fig. 7) show that the RMS difference and bias drastically increase with height above 4 km. For JFM, the RMS difference at 4 km is 2.37 K with an average of 1.92 K for the bottom 4 km. Above the height of 4 km, the RMS difference increases to 6.20 K at 10 km. Similarly, AMJ has an average RMS difference of 1.95 K below 4 km and a RMS difference of 1.65 K at 4 km, which increases to a maximum of 5.64 K at 9.5 km. For JAS, the lower 4 km has a higher average RMS difference of 2.76 K, with 3.47 K at 4 km. The RMS difference increases only to 4.93 K at 6 km and remains above 4 K up to 10 km. OND has an average value of 2.46 K for the lower 4 km and drastically increases from 4 to 6 km with a maximum value of 5.07 K. The RMS difference then decreases to 3.29 K at 10 km. Each season shows, on average, a moderate increase with height in the RMS difference below 4 km. Below 4 km the RMS difference and bias show a difference of 3 K or less, except for JAS, which is 4 K or less. For all seasons the rate of increase for the RMS difference above 4 km was drastic. This indicated that the MWRP data above 4 km should be viewed with skepticism.

The RMS difference and bias profiles for the absolute humidity were calculated for each season (Fig. 7, right column). The absolute humidity has a much smaller RMS difference in winter than in any other season; this is to be expected because of the very low absolute humidity values that are characteristic of the dry winter climate in the High Arctic. Note that the absolute humidity calculated from the Clausius–Clapeyron equation would lead to having lower RMS differences at colder temperatures.

The RMS difference and bias profiles for the three sea ice concentration categories for 0–2 km are given (Fig. 8). These RMS and bias calculations are restricted to the lowest 2 km because the characteristics of the surface should only impact the atmospheric boundary layer and not the entire profile (Overland and Guest 1991).

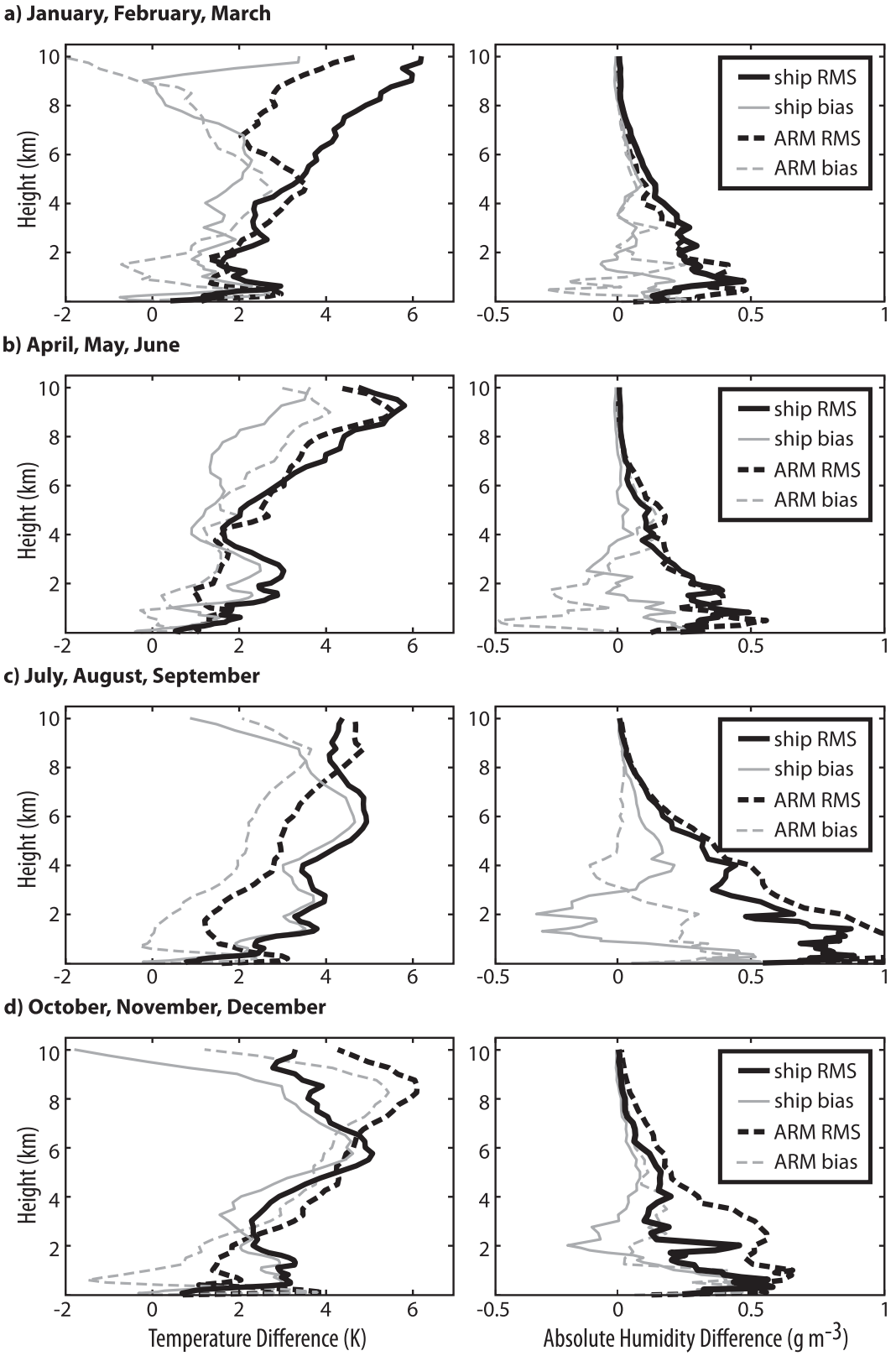

FIG. 7. The RMS difference, and bias vs height (km) for (left) temperature profiles and (right) absolute humidity. The bias was determined by the raobs minus the MWRP. The RMS difference and bias from the ship (solid lines) and the RMS difference and base calculated from Barrow (dashed lines) are shown. For all seasons the Barrow RMS difference (bias) was statistically similar to the ship's RMS difference (bias).

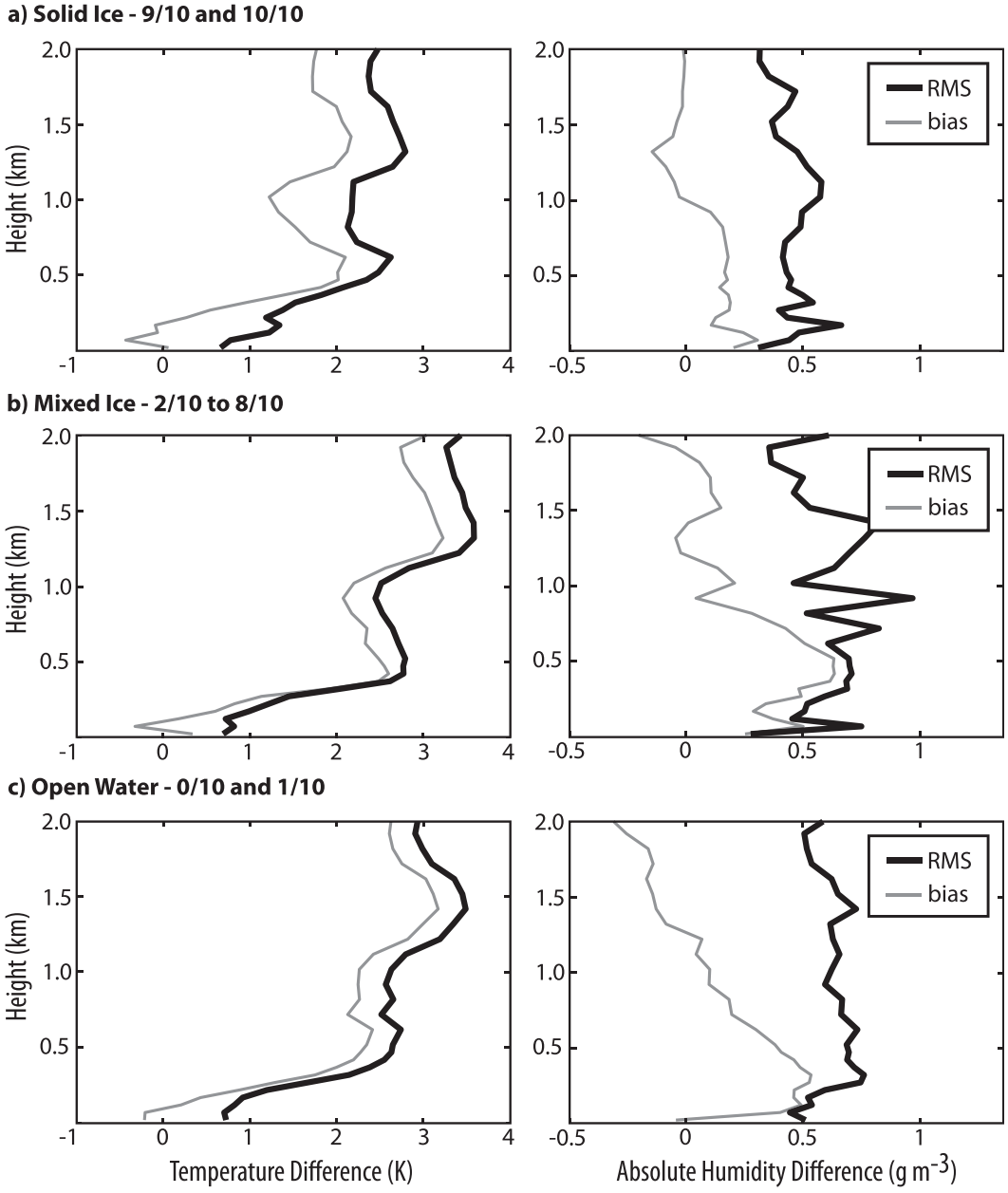

FIG. 8. The root-mean-square difference, and bias vs height (km) for (left) temperature profiles and (right) absolute humidity. The data were categorized by sea ice concentration. The bias was determined by the raobs minus the MWRP.

The RMS difference and bias for absolute humidity over close pack ice is generally smaller than over mixed ice or open water (Fig. 8, right column). The RMS difference for absolute humidity over close pack ice stays around 0.5 g m^{-3}, whereas over mixed ice the RMS difference is much more varied and has a range from 0.25 to 1.0 g m^{-3} in the lower 2 km. Over open ocean the absolute humidity is less varied than over mixed ice, but is still generally larger than over close pack ice, with a range from approximately 0.5 to 0.75 g m^{-3}. The RMS for absolute humidity is the same order of magnitude as previous studies in Barrow, where Liljegren et al. (2001) found the RMS differences to be about 0.5 g m^{-3} near the surface.

When the RMS difference and bias profiles are categorized by sea ice concentration, the mean temperature biases are consistently positive for all sea ice groups with a small exception near the surface (Fig. 8, left column).

When there is very little open water, 9/10ths or 10/10ths sea ice concentration, the mean RMS and bias stays below 3 K. For both open water and mixed sea ice concentrations the RMS and bias remains below 4 K up to 2 km in height. There is not a significant difference between the RMS and bias for open water, mixed sea ice, and solid ice, below 2 km, when compared to the seasonal data. This indicates that the MWRP can reliably measure the boundary layer over varied sea ice concentrations.

Focusing on the lower 2 km, which are generally influenced by the nature of the underlying surface, RMS differences for temperature averaged 1.79 K through the lowest 2 km for JFM, 1.81 K for AMJ, 2.51 K for JAS, and 2.47 K for OND. Average biases of +0.99, +1.19, +2.13, and +2.08 K, respectively, indicate that the MWRP measurements were colder than the raobs for the lower 2 km. The RMS difference for absolute humidity averaged 0.25 g m^{-3} in the lowest 2 km during JFM, 0.32 g m^{-3} for AMJ, 0.74 g m^{-3} for JAS, and 0.37 g m^{-3} for OND. Average biases of +0.08 g m^{-3} for profiles over 9/10ths and 10/10ths sea ice concentration, +0.26 g m^{-3} for profiles over 2/10ths–8/10ths concentrations, and +0.16 g m^{-3} over 0/10ths and 1/10th concentrations, indicated that the MWRP measurements were slightly drier than the raobs for the lower 2 km.

c. Comparisons with Barrow

The RMS difference and bias was also calculated for each season and height level using the data from ARM's Barrow location (Fig. 7). The Mann–Whitney two-sided rank sum test was performed on the RMS difference (bias) between the ship and Alaska for each season. A p value of less than 0.05 indicated that the RMS difference (bias) at the two locations has unequal medians or is statistically different. A p value of greater than 0.05 fails to reject the null hypothesis of equal medians, indicating that the RMS difference (bias) is statistically similar. When comparing the temperature RMS difference between the ship's location and Barrow, each season had p values greater than 0.05, indicating that the RMS difference for temperature from the ship is statically similar to the RMS difference for Barrow. The results were the same for the temperature bias with each season having a p value greater than 0.05, again indicating that the bias for the ship's MWRP is statistically similar to the bias for the MWRP at Barrow. The absolute humidity RMS difference (bias) p values were again greater than 0.05, which shows that the absolute humidity RMS difference (bias) for the MWRP on board the ship is statistically similar to that in Barrow.

For all seasons and both temperature and absolute humidity the RMS difference (bias) for the ship is statistically similar to the RMS difference (bias) for Barrow. This indicates that our MWRP performs as well as ARM's MWRP stationed in Barrow.

d. Frequency distribution

The frequency distribution of the case-to-case differences was plotted (Fig. 9). The case-to-case differences, raobs minus MWRP, were calculated for each of the 68 atmospheric profiles. The data were grouped into five classes with heights of (a) 0–0.1, (b) 0.4–0.5, (c) 0.9–1.1, (d) 4.75–5.25, and (e) 9.5–10 km. Each height class contained 204 bias measurements. For both temperature and absolute humidity, the data were divided into class intervals with a width 0.5, where from −0.25 to 0.25 is defined as the 0 interval. If the sample was large enough and the errors were random, the frequency distributions would be normal and centered on zero. Looking at the temperature distribution (left column in Fig. 9), all height levels exhibit an obvious positive skewness, with the exception of the 9.5–10-km level. The 9.5–10-km level does have a positive skewness, although the distribution curve is multimodal. The absolute humidity distribution (right column in Fig. 9) also shows an obvious positive skewness, with every height level clearly centered with a positive bias.

Having a relatively large sample of 204 measurements and generally a positive skewed distribution indicates that the errors are systematic. The temperature distribution with a positive skewness indicates that the MWRP has a systematic cold bias compared to the raobs. Similarly, the positive skewness for the absolute humidity indicates that the MWRP has a systematic dry bias compared to the raobs. This could be due to the MWRP having a neural network that was trained with data from land-based radiosondes. The microwave radiometer profiles may exhibit a dry bias more akin to the climate conditions found at Inuvik, rather than a marine climate.

5. Case study

A warm front passed over the study area between 25 and 27 July 2009. Five radiosondes were released at intervals of 10–14 h, creating a profiled time series of the evolution of the system over of the study area. Because the measurements from both the raobs and MWRP were taken on board a ship that was mobile with an average speed of 3.8 kt, the analyzed warm front was not geospatially accurate. During the passage of this warm front, the surface temperatures increased from 0.6°C at 1200 UTC 25 July to a maximum of 5.3°C at 0300 UTC 27 July. No precipitation was recorded during the event; however, the recorded cloud cover ranged from 0/8ths to 8/8ths. With the warm front a surface inversion was present; the

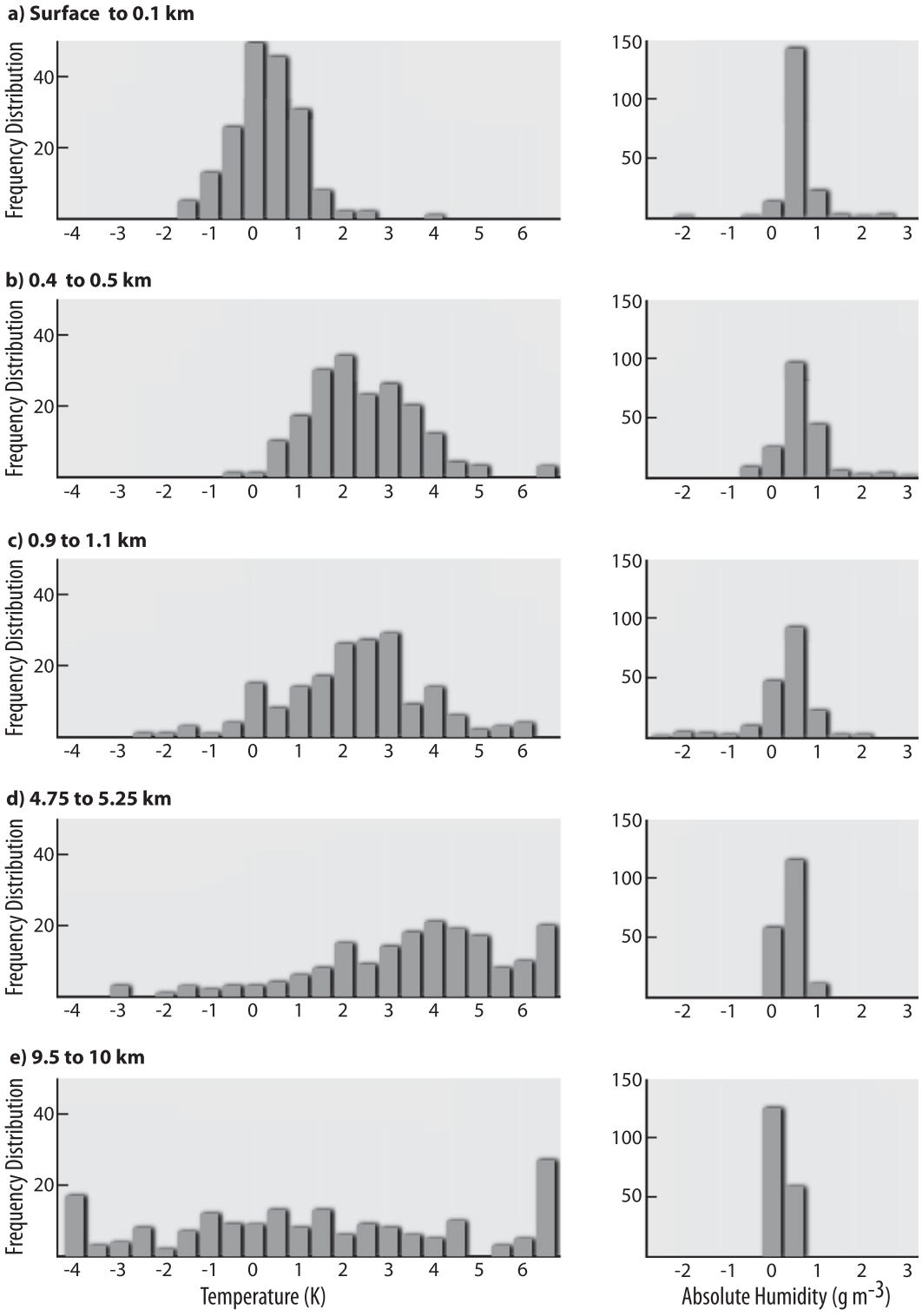

FIG. 9. The frequency distribution of the case-to-case differences (raobs minus the shipborne MWRP). The data were grouped by heights: (a) 0–0.1, (b) 0.4–0.5, (c) 0.9–1.1, (d) 4.75–5.25, and (e) 9.5–10.0 km. Generally a positive skewed temperature distribution is shown, indicating a systematic cold bias compared to the raobs. The positive skewness of the absolute humidity indicates a systematic dry bias of the MWRP compared to the raobs.

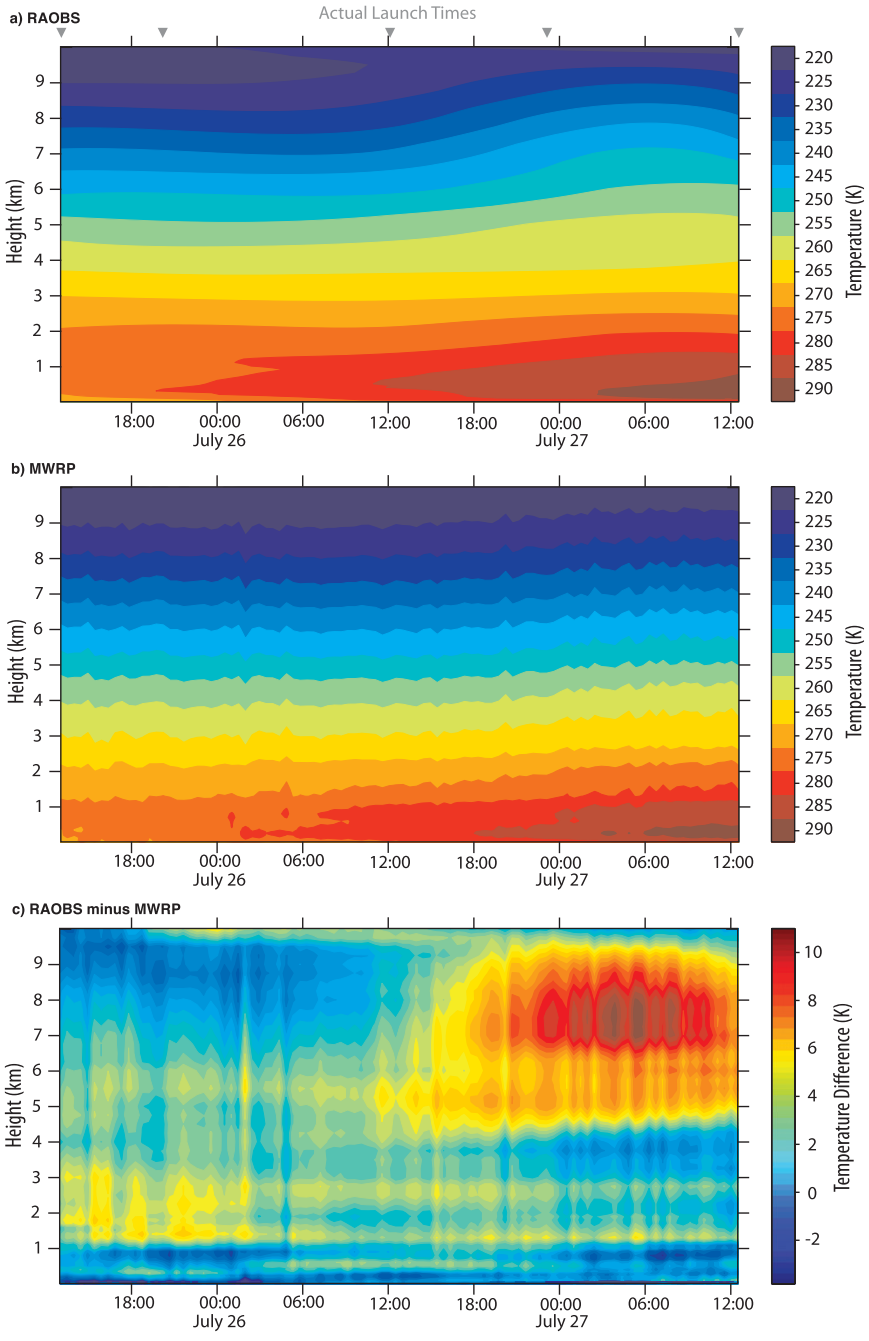

FIG. 10. The radiosonde temperature data from five launches was calculated using a cubic spline interpolation over the period from 1245 UTC 25 Jul 2009 until 1247 UTC 27 Jul 2009 as shown in Fig. 6a. Figure 6b shows the raw MWRP data from that same time period while Fig. 6c shows the difference between the two, raobs − MWRP.

inversion had a difference of 15°C between the surface and approximately 1 km, which later strengthened to 21°C.

Figures 10 and 11 show the temperature and absolute humidity profiles during the 48-h time period starting at 1245 UTC 25 July 2009. Figure 10a shows the temperature as interpreted from the five radiosonde profiles. Intermediate temperature values were calculated using a cubic spline interpolation at intervals of 28.8 min for every height level given by the MWRP. Figure 10b shows the raw data from the MWRP using the data with the nearest time to the 28.8-min interval. An attempt was made to use the 1-min data from the MWRP to compare

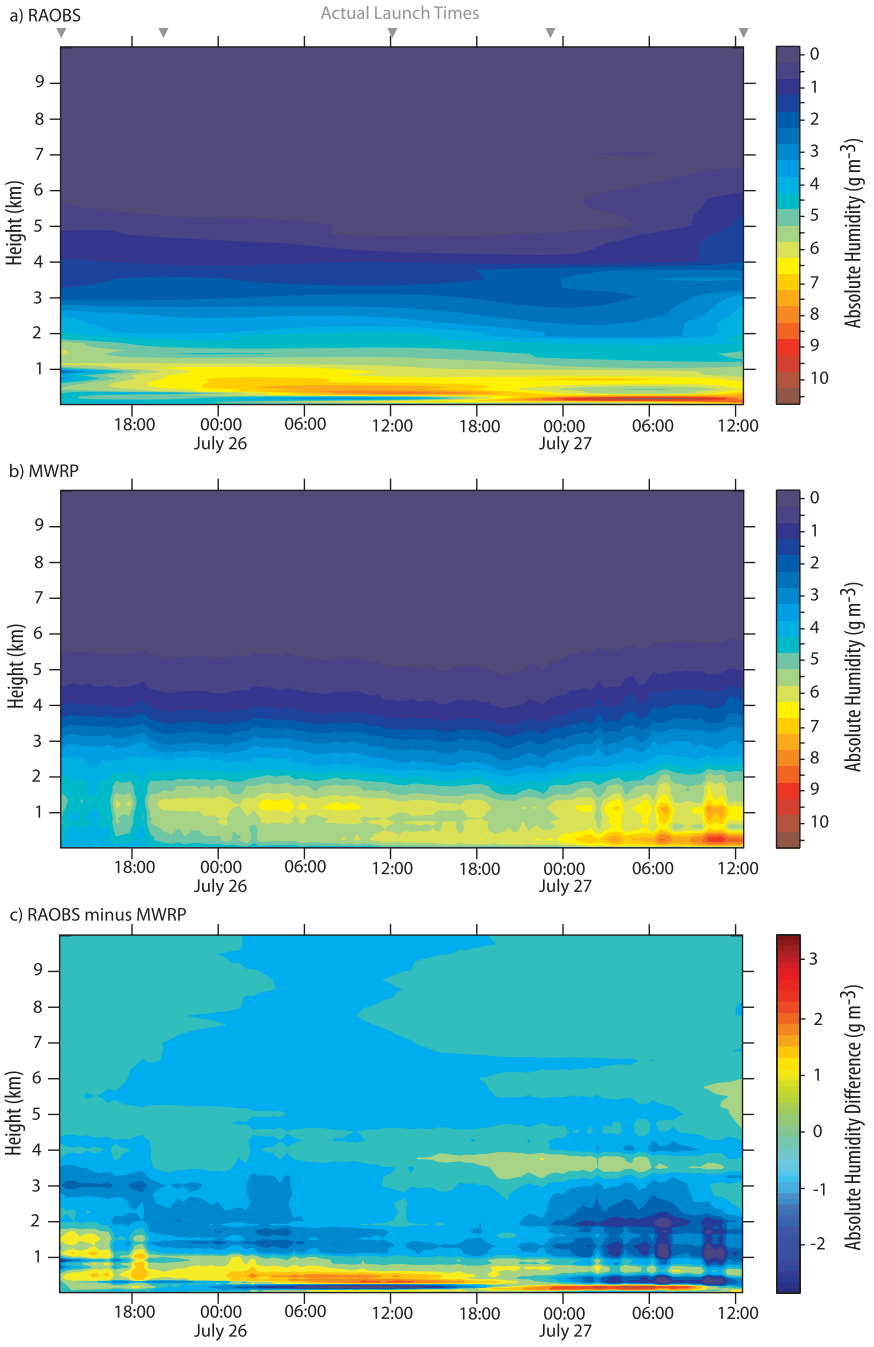

FIG. 11. As in Fig. 6, but for absolute humidity.

to 1-min data created using the cubic spline interpolation from the raobs; however, when plotted the spacing between the data points was so fine it really was indistinguishable from the 28.8-min data points. Figure 10c shows the difference between the two—the raobs minus the MWRP. Figure 11 was calculated in the same manner as Fig. 10, except for absolute humidity rather than temperature.

Initially there is an apparent similarity between the raobs and MWRP temperature measurements at all heights, with the best results below 1 km (Fig. 10). At approximately 1800 UTC July 26 a discrepancy begins between the two instruments, where the difference between raobs and the MWRP above 5 km can be substantial (up to 10 K). A similar, but much more subtle, difference in absolute humidity is also noted for the

same altitude and timeframe (Fig. 11). This difference may be due to a discrepancy in the capability of the MWRP to resolve the modification of absolute humidity and temperature profiles by forced convection along an advancing front. During the passage of the warm front (Figs. 10 and 11), warmer, less dense air from behind the front was forced to ascend over the cooler, denser air ahead of the front. Images from the all-sky camera mounted on board the CCGS *Amundsen* show cumulus clouds over the area from about 0100 to 1200 UTC 27 July 2009. The ceilometer data indicate that the cloud height ranged from 1000 to 1700 m during the same time. Moisture was apparently forced vertically, which is evident in the development of a moisture plume at the 2–3-km altitude range (Fig. 11). The plume builds in magnitude most notably from 0000 to 1200 UTC 27 July 2009, where the absolute humidity increased on average by 0.68 g m^{-3}, from the previous 12 h, and corresponded with the large difference between the MWRP and raobs measurements.

Looking at Fig. 11, there is again a similarity between the general pattern of the raobs measurements for absolute humidity and the MWRP measurements. Figure 11c shows that there is little difference between the raobs and the MWRP measurements above 5 km; this is not surprising because the humidity drops to near zero. The MWRP shows the increase in moisture from the warm front; however, there are differences between the raobs and MWRP near the surface. This may be due to the MWRP being trained with profiles from Inuvik, that is, over land, rather than over the ocean where the MWRP was deployed.

In a recent study, Knupp et al. (2009) determined that MWRP's are capable of providing considerable detail on the rapidly changing thermodynamic structure of transitioning boundaries. The high temporal resolution was able to resolve detailed mesoscale thermodynamic and limited microphysical features from various dynamic weather phenomena, including a complex cold front, a nocturnal bore, and a squall line. Although the cubic spline interpolation used in this case study for the raobs is only an estimate of what occurred, the MWRP mounted on board a ship in the Arctic was capable of capturing the general changes that occurred rapidly with the transitioning boundary of the warm front.

6. Vertical resolution

The vertical resolution defined by Smith et al. (1999) is given by the half-width of the interlevel covariance matrix [Eq. (1)]. Both Smith et al. (1999) and Guldner and Spankuch (2001) suggest that this method gives the lower limit of the vertical resolution. Through case studies, Guldner and Spankuch (2001) show that the MWRP has a higher vertical resolution than the interlevel covariance method suggests,

$$C(z_0, z) = \frac{\sum_{i=1}^{N} [T_r(z_0) - T(z_0)][T_r(z) - T(z)]}{\sqrt{\sum_{i=1}^{N} [T_r(z_0) - T(z_0)]^2 \sum_{i=1}^{N} [T_r(z) - T(z)]^2}}. \quad (1)$$

Equation (1) gives the vertical interlevel covariance for temperature, where N is the number of MWR and raob profile comparisons, T_r is the temperature from the MWRP, T is the temperature from the raobs, z is the height, and z_0 is the reference height for which the vertical resolution is being defined. Vertical resolution is defined as the half-width of the covariance function for each measured height.

The vertical resolution for temperature had a skewed error covariance, which affected the estimate of the vertical resolution. This may be due to the vertical resolution being calculated with only 68 profiles collected over a 2-yr time period. Before calculating the vertical resolution, the bias was removed from the MWRP data based on sea ice concentration, as the method defined by Smith et al. (1999) requires. Figure 12 shows the vertical resolution of temperature and absolute humidity of the MWR profiles for up to 8 km in height.

As shown in Fig. 12, the lower limit of the resolution degrades more slowly for the absolute humidity than for temperature. The vertical resolution for temperature degrades substantially above 1.5 km to a minimum value of 4750 m at 4 km, and then increases to 3250 m at 8 km. The vertical resolution for absolute humidity stays below 1000 m up to 2 km, and there is a significant degradation from 1000 to 3000 m in the resolution between approximately 3.5 and 5 km.

Westwater et al. (2000) found the resolution of an MWRP located at Barrow to have a similar result to the shipborne MWRP. The resolution for temperature was approximately equal to the height up to an altitude of 2.5 km where the resolution was found to be approximately 3.5 km. Cimini et al. (2006) found the vertical resolution for temperature measurements to be about half the altitude from 0 to 3 km, and for water vapor measurements the resolution was found to be 500 m from the surface to about 1.5 km, then increasing to about 1 km at an altitude of 2.5 km. They found that the MWRP would normally identify the existence of a significant temperature inversion below 1 km, but would have difficulty in identifying inversions at heights above 1 km. From a MWRP–radiosonde comparison at Payerne, Hewison et al. (2004)

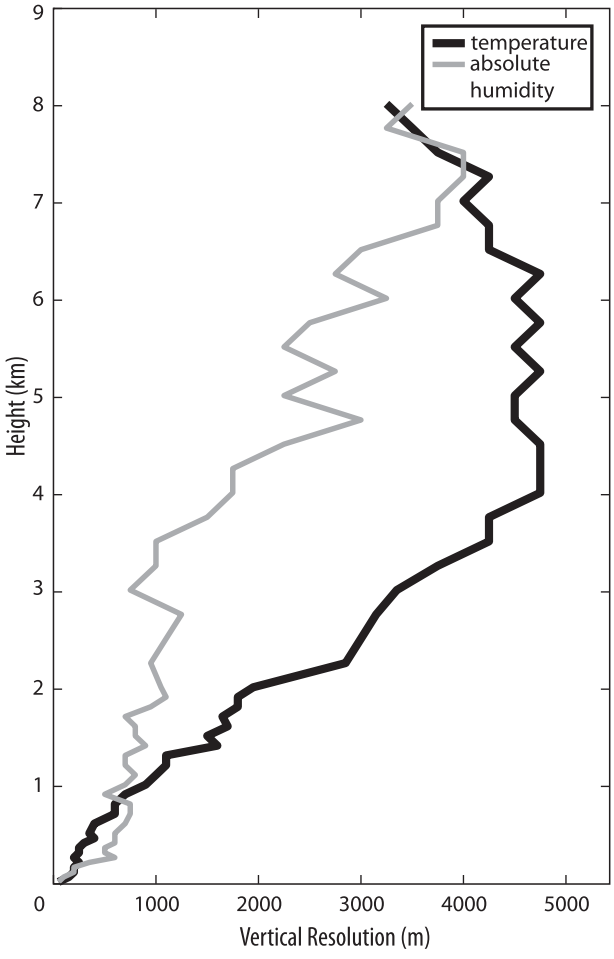

FIG. 12. The vertical resolution of the MWRP (m) against height (km) as calculated by the interlevel covariance method.

found that the Radiometrics zenith algorithm tended to retrieve temperature inversions with the correct amplitude, but often overestimated their depth because of the limits of the instrument's vertical resolution. Cadeddu et al. (2002) analyzed the MWRP resolution for temperature using a multiresolution wavelet transform, and found that at an altitude of up to 400 m the resolution was 125 m. At an altitude of 1.5 km the resolution was 500 m. Cadeddu et al. (2002) compared their results to that of Guldner and Spankuch (2001) who found lower resolutions of 500 m at an altitude of 300 m, degrading to 1 km at an altitude of 500 m. Cadeddu et al. (2002) found that their resolutions agreed better with the RMS difference analysis done by Guldner and Spankuch (2001). They concluded that the radiometer should be able to detect the structures in the profile at higher altitudes based on their analysis.

As suggested by Smith et al. (1999) and Guldner and Spankuch (2001), the interlevel covariance method of calculating the vertical resolution is a lower limit. The previous statistical analyses of the data and the case study lead to the conclusion that the vertical resolution of the MWRP is much greater than that indicated by the interlevel covariance method.

7. Discussion and conclusions

A total of 68 radiosonde profiles were used to verify corresponding radiometer profiles. The dataset collected on board the CCGS *Amundsen* is extremely unique. The two field campaigns in 2008 and 2009 collected high temporal data for humidity and temperature, spanning every season. All data were collected in the Arctic marine environment for a variety of different surface types, from open ocean to closed pack ice. Other field campaigns in the Arctic have lacked the breadth spatially and temporally, generally concentrating on a single location close to shore and over a short summer field season. The data collected from 2008 and 2009 are an invaluable resource.

The 68 profiles were grouped by underlying sea ice concentrations and season. There appears to be a large bias for both temperature and absolute humidity when there are low concentrations of sea ice present. Higher concentrations of sea ice act as a barrier reducing the transfer of heat and moisture between the ocean and the atmosphere (Barry et al. 1993); therefore, lower concentrations of sea ice may result in more moisture in the Arctic marine atmosphere. The large bias with low concentrations of sea ice is not unexpected because the MWRP employs a neural network that is trained using historical land-based radiosondes. Because of the limited spatial and temporal radiosonde history in this region, radiosonde data from Inuvik were employed. This may have introduced a bias close to the surface in the neural network coefficients, and may have lead the MWRP to exhibit a dry bias, akin to the climate conditions found at Inuvik, rather than a marine climate.

The Mann–Whitney two-sample difference test was performed on historical Inuvik radiosondes from 2002 to 2006, and the 2008 and 2009 radiosondes launched over the Beaufort Sea on board the CCGS *Amundsen*. The Mann–Whitney two-sample difference test indicated that the data collected over the Beaufort Sea were generally not statistically similar to the historical Inuvik data, with the exception of JFM and OND when the Beaufort Sea had high concentrations of sea ice present. This further indicates that the MWRP bias is likely affected by the neural network being trained with historical Inuvik radiosonde data.

RMS differences for temperature (raobs − MWRP) averaged 1.79 K through the lowest 2 km for the winter (JFM) season, 1.81 K for the spring (AMJ) season,

2.51 K for the summer (JAS) season, and 2.47 K for the fall (OND) season. Average biases of +0.99, +1.19, +2.13, and +2.08 K, respectively, indicate that the MWRP measurements were colder than the raobs for the lower 2 km. Similarly, biases for the upper 2–8 and 8–10 km were all positive, again indicating that the MWRP consistently recorded lower temperatures than the raobs. However, the shipborne MWRP data were statistically compared to the shipborne raobs using the Wilcoxon match pair test. When the two datasets are statistically similar, this indicates that the two instruments are measuring from the same population or same air parcel. For temperature, from above 200–250 m to approximately 5–9 km, the MWRP and raobs are statistically similar, again indicating that they are measuring from the same population. With the exception of JAS, from the surface to approximately 1.2 km, they are not statistically similar.

The RMS differences (bias) were statistically compared to RMS differences (bias) from Barrow. The Mann–Whitney two-sided rank sum test was performed on the two locations. For each season and both temperature and absolute humidity, the RMS differences (bias) from the shipborne MWRP were statistically similar to the RMS differences (bias) from the Barrow MWRP. This indicated that the shipborne MWRP performed as well as the terrestrially based Barrow MWRP.

The RMS difference for absolute humidity (raobs − MWRP) averaged 0.25 g m^{-3} in the lowest 2 km during the winter (JFM) season, 0.32 g m^{-3} for the spring (AMJ) season, 0.74 g m^{-3} for the summer (JAS) season, and 0.37 g m^{-3} for the fall (OND) season. Average biases of +0.08 g m^{-3} for profiles over $^{9}/_{10}$ths and $^{10}/_{10}$ths sea ice concentration, +0.26 g m^{-3} for profiles over mixed sea ice concentrations ($^{2}/_{10}$ths–$^{8}/_{10}$ths), and +0.16 g m^{-3} for over open water ($^{0}/_{10}$ths and $^{1}/_{10}$th), indicated that the MWRP measurements were slightly drier than the raobs for the lower 2 km. The sea ice concentrations of $^{9}/_{10}$ths and $^{10}/_{10}$ths have the lowest bias, which is to be expected with the least amount of open water present. When the shipborne MWRP data were statistically compared to the shipborne raobs using the Wilcoxon match pair test for absolute humidity, the data were generally statistically different, indicating that the microwave profiler and radiosonde data were from two different populations.

The vertical resolution was calculated using the interlevel covariance method as defined by Smith et al. (1999). The calculated vertical resolutions were, in general, as coarse as the height measured; at a height of 1 km the vertical resolution was approximately 1000 m. This could be a result of the dataset being limited to only 68 profiles and the resulting covariance curves that were skewed rather than bell shaped. Although currently this is the only method available, we concluded that the resolutions given are far too coarse compared to the resolution suggested by the statistical analysis of the individual seasons and as shown in the case study.

The RMS differences for temperature in the lower 2 km were between 1.5 and 2.5 K; similarly, Liljegren et al. (2001) found RMS differences of 1–2 K for temperature at Oklahoma, Kansas, and Barrow. The RMS differences for absolute humidity were 0.25–0.74 g m^{-3}, similar to the average RMS difference of 0.5 g m^{-3} found by Liljegren et al. (2001) at Barrow. The MWRP aboard the CCGS *Amundsen* had little calibration drift over time; however, an internal blackbody bias on the order of 0.5 K likely contributed to the consistent cold bias. The MWRP mounted on board a ship at sea would also be sensitive to the pitch and roll motions of the ship, leading to a greater error relative to land-based locations. The inherent measurement errors in radiosondes, 0.5 K for temperature and 10% for relative humidity (Pratt 1985; Schmidlin 1988; Miloshevich et al. 2006), and the drift of the balloons from zenith make them less than ideal references (Guldner and Spankuch 2001). On a mobile ship in the Arctic the drift would be exaggerated by the movement of the ship relative to the wind speed and direction.

The objective of this paper was to determine how reliable the MWRP was when mounted on board a mobile ship in the High Arctic. Although the MWRP had difficulty with forced convection along an advancing front and with near-surface humidity, as seen in the case study, the data retrieved from the MWRP appear suitable for measuring lower-level boundary layer temperature and absolute humidity profiles. Based on the comparison of the MWRP with the raobs and the case study we conclude that the MWRP generally gives reliable measurements of both parameters. The bias and RMS difference of the lower 4 km, for both temperature and absolute humidity, were of the same order of magnitude as those found in Alaska (Liljegren et al. 2001). When comparing the RMS difference and bias from the same time period, the shipborne MWRP was statistically similar to the Barrow MWRP. This study indicates that MWRP data collected in future studies of the boundary layer in the Beaufort Sea and Amundsen Gulf region will reliably measure the temperature and humidity profiles, and the profiles will capture both seasonal variations, as well as trends over short time scales, such as those found in case studies.

Acknowledgments. This work was funded by the Natural Sciences and Engineering Research Council (NSERC), the International Polar Year (IPY) Federal

Program Office, and the Canada Research Chairs (CRC) programs through grants to D. G. Barber. Thanks to C. R. Candlish, A. C. Coates, J. Iacozza, and R. Scharien for their contributions. We would like to acknowledge the tireless efforts of the captain and crew of the CCGS *Amundsen*. We would like to acknowledge the U.S. Department of Energy as part of the Atmospheric Radiation Measurement (ARM) Climate Research Facility; data from North Slope Alaska were used.

REFERENCES

Barber, D. G., M. G. Asplin, Y. Gratton, J. V. Lukovich, R. J. Galley, R. L. Raddatz, and D. Leitch, 2010: The International Polar Year (IPY) circumpolar flaw lead (CFL) system study: Overview and the physical system. *Atmos.–Ocean,* **48,** 225–243.

Barry, R., M. Serreze, J. Maslanik, and R. Preller, 1993: The arctic sea ice-climate system: Observations and modeling. *Rev. Geophys.,* **31,** 397–422.

Cadeddu, M., G. Peckham, and C. Gaffard, 2002: The vertical resolution of ground-based microwave radiometers analyzed through a multiresolution wavelet technique. *IEEE Trans. Geosci. Remote Sens.,* **40,** 531–540.

Cimini, D., T. Hewison, L. Martin, J. Guldner, C. Gaffard, and F. Marzano, 2006: Temperature and humidity profile retrievals from ground-based microwave radiometers during TUC. *Meteor. Z.,* **15,** 45–56.

——, E. Westwater, A. Gasiewski, M. Klein, V. Leuski, and S. Dowlatshahi, 2007: The ground-based scanning radiometer: A powerful tool for study of the arctic atmosphere. *IEEE Trans. Geosci. Remote Sens.,* **45,** 2759–2777.

Gaffard, C., J. Nash, E. Walker, T. J. Hewison, J. Jones, and E. G. Norton, 2008: High time resolution boundary layer description using combined remote sensing instruments. *Ann. Geophys.,* **26,** 2597–2612.

Guldner, J., and D. Spankuch, 2001: Remote sensing of the thermodynamic state of the atmospheric boundary layer by ground-based microwave radiometry. *J. Atmos. Oceanic Technol.,* **18,** 925–933.

Hewison, T., 2007: 1D-VAR retrieval of temperature and humidity profiles from a ground-based microwave radiometer. *IEEE Trans. Geosci. Remote Sens.,* **45,** 2163–2168.

——, C. Gaffard, J. Nash, D. Ruffieux, R. Nater, H. Berger, M. Perroud, and B. Andrade, 2004: Monitoring inversions from ground-based remote sensing instruments during temperature, humidity, and cloud profiling campaign (TUC). *Proc. Eighth Specialist Meeting on Microwave Radiometry and Remote Sensing Applications,* Rome, Italy, University La Sapienza. [Available online at http://www.radiometrics.com/microRad04_Hewison.pdf.]

Knupp, K., T. Coleman, D. Phillips, R. Ware, D. Cimini, F. Vandenberghe, J. Vivekanandan, and E. Westwater, 2009: Ground-based passive microwave profiling during dynamic weather conditions. *J. Atmos. Oceanic Technol.,* **26,** 1057–1073.

Kwok, R., and G. Cunningham, 2010: Contribution of melt in the Beaufort Sea to the decline in arctic multiyear sea ice coverage: 1993–2009. *Geophys. Res. Lett.,* **37,** L20501, doi:10.1029/2010GL044678.

Liljegren, J., B. Lesht, S. Kato, and E. Clothiaux, 2001: Initial evaluation of profiles of temperature, water vapor and cloud liquid water from a new microwave profiling radiometer. *Proc. Fifth Symp. on Integrated Observing Systems,* Albuquerque, NM, Amer. Meteor. Soc., 8.6. [Available online at http://www.radiometrics.com/ams01.pdf.]

Markus, T., J. C. Stroeve, and J. Miller, 2009: Recent changes in arctic sea ice melt onset, freezeup, and melt season length. *J. Geophys. Res.,* **114,** C12024, doi:10.1029/2009JC005436.

Maslanik, J. A., C. Fowler, J. Stroeve, S. Drobot, J. Zwally, D. Yi, and W. Emery, 2007: A younger, thinner Arctic ice cover: Increased potential for rapid, extensive sea-ice loss. *Geophys. Res. Lett.,* **34,** L24501, doi:10.1029/2007GL032043.

——, J. Stroeve, C. Fowler, and W. Emery, 2011: Distribution and trends in Arctic sea ice age through spring 2011. *Geophys. Res. Lett.,* **38,** L13502, doi:10.1029/2011GL047735.

Maykut, G., 1978: Energy exchange over young sea ice in the central arctic. *J. Geophys. Res.,* **83** (C7), 3646–3658.

Miloshevich, L., H. Vomel, D. Whiteman, B. Lesht, F. Schmidlin, and F. Russo, 2006: Absolute accuracy of water vapor measurements from six operational radiosonde types launched during AWEX-G and implications for AIRS validation. *J. Geophys. Res.,* **111,** D09S10, doi:10.1029/2005JD006083.

Overland, J. E., and P. S. Guest, 1991: The arctic snow and air temperature budget over sea ice during winter. *J. Geophys. Res.,* **96** (C3), 4651–4662.

Pratt, R., 1985: Review of radiosonde humidity and temperature errors. *J. Atmos. Oceanic Technol.,* **2,** 404–407.

Radiometrics, 2008: MP-3000A profiler operator's manual. 87 pp.

Rothrock, D., Y. Yu, and G. Maykut, 1999: Thinning of the arctic sea-ice cover. *Geophys. Res. Lett.,* **26** (23), 3469–3472.

Schmidlin, F., 1988: WMO international radiosonde comparison—Phase II, Wallops Island (USA), 1985. Instruments and Observing Methods Rep. 29, 113 pp.

Smith, W. L., W. F. Feltz, R. O. Knuteson, H. E. Revercomb, H. M. Woolf, and H. B. Howell, 1999: The retrieval of planetary boundary layer structure using ground-based infrared spectral radiance measurements. *J. Atmos. Oceanic Technol.,* **16,** 323–333.

Solheim, F., J. R. Godwin, E. R. Westwater, Y. Han, S. J. Keihm, K. March, and R. Ware, 1998: Radiometric profiling of temperature, water vapor, and cloud liquid water using various inversion methods. *Radio Sci.,* **33,** 393–404.

Turner, J., J. Overland, and J. Walsh, 2007: An arctic and antarctic perspective on recent climate change. *Int. J. Climatol.,* **27,** 277–293.

Ware, R., R. Carpender, J. Guldner, J. Liljegren, T. Nehrkorn, F. Solhelm, and F. Vandenberghe, 2003: A multichannel profiler of temperature, humidity, and cloud liquid. *Radio Sci.,* **38,** 1–44.

Westwater, E., Y. Han, and F. Solheim, 2000: Resolution and accuracy of a multi-frequency scanning radiometer for temperature profiling. *Microwave Radiometry and Remote Sensing of the Earth's Surface and Atmosphere,* P. Pampaloni and S. Paloscia, Eds., VSP, 129–135.